

Learning to Build Shapes by Extrusion

Thor V. Christiansen
 Technical University of Denmark
 Kongens Lyngby, Denmark
 tdvc@dtu.dk

Karan Singh
 University of Toronto
 Toronto, Canada
 karan@dgp.toronto.edu

Karran Pandey
 University of Toronto
 Toronto, Canada
 karran@cs.toronto.edu

Morten R. Hannemose
 Technical University of Denmark
 Kongens Lyngby, Denmark
 mohan@dtu.dk

Alba Reinders
 Technical University of Denmark
 Kongens Lyngby, Denmark
 albre@dtu.dk

J. Andreas Bærentzen
 Technical University of Denmark
 Kongens Lyngby, Denmark
 janba@dtu.dk

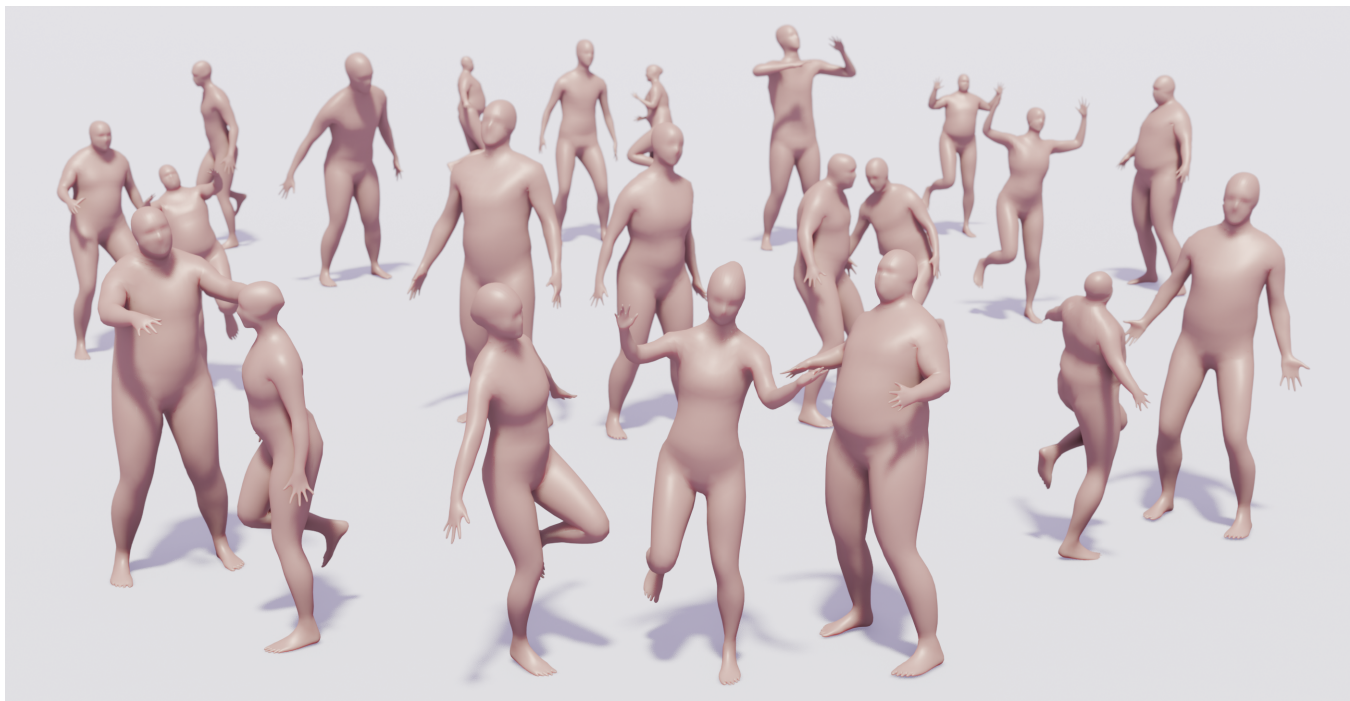


Figure 1: Random generations of upper bodies of the DFAUST dataset with our finetuned Llama LLM.

Abstract

We introduce Text Encoded Extrusion (TEE), a text-based representation that expresses mesh construction as sequences of face extrusions rather than polygon lists, and a method for generating 3D meshes from TEE using a large language model (LLM). By learning extrusion sequences that assemble a mesh, similar to the way artists create meshes, our approach naturally supports arbitrary output face counts and produces manifold meshes by design, in contrast to recent transformer-based models. The learnt extrusion sequences can also be applied to existing meshes - enabling editing in addition to generation. To train our model, we decompose a library of quadrilateral meshes with non-self-intersecting face loops into constituent loops, which can be viewed as their building blocks, and finetune an LLM on the steps for reassembling the meshes by performing a sequence of extrusions. We demonstrate that our representation enables reconstruction, novel shape synthesis, and the addition of new features to existing meshes.

CCS Concepts

- Computing Methodologies → Mesh models.

Keywords

Face Extrusion Quad meshes, extrusions, LLM

1 Introduction

Learning-based models for 3D shape generation have achieved incredible results over the last few years [16, 17, 25, 28], generating a wide variety of detailed 3D shapes. However, most of these methods rely on implicit surface representations, which struggle with learning sharp features. Moreover, the methods often produce overly dense triangle meshes when extracting surfaces from neural fields, as a byproduct of iso-contouring methods such as Marching Cubes [19] and its variants [6, 11, 35]. This is a problem, as a

compact 3D mesh is often the desired output for downstream applications like computer games or video animations. To tackle these issues, a recent line of work based on transformers [41] has been proposed. Similar to natural language processing with transformers, these methods generate the primitives of a mesh sequentially, thereby learning the mesh directly rather than an implicit representation. This is advantageous, as artists often desire control over the structure of the polygonal mesh, something that is not provided by an iso-surface. On the other hand, these recent methods produce relatively coarse meshes [5, 40]. By representing every single mesh primitive as a token (whether it be the vertex positions and/or the polygonal faces), the sequence length of a moderately high-resolution mesh becomes critically long since most transformer models have a limited context window, which, in turn, is because the attention mechanism often scales quadratically with the sequence length. Moreover, transformers typically generate a discrete probability distribution over output tokens to predict the next token. This makes it difficult for them to predict continuous quantities, such as the coordinates of mesh vertices. As a result, many current methods [5, 9, 37] restrict the vertex positions to a predefined spatial grid. Finally, because shapes are generated sequentially, many methods only produce a soup of primitives rather than a connected mesh.

To address these challenges, we propose learning to build a mesh through a sequence of extrusions rather than directly learning the sequence of polygons that form the mesh. Our method can reproduce entire meshes, explore variations, and modify existing shapes.

Rather than devising a network architecture for learning sequences of extrusions, we convert the extrusion commands to text, Text Encoded Extrusions (TEE), and learn sequences of extrusions through fine-tuning an existing large language model (LLM). Our approach has several advantages; in particular, it imposes no limit on the level of detail of the output mesh and ensures that we always obtain a mesh with the expected connectivity, since this is enforced by the extrusion operations. With our extrusion framework, we can also add features to existing meshes.

Finally, it gives us complete freedom to choose the LLM.

In summary, our main contributions are:

- A learning-based methodology for generating 3D meshes via sequences of extrusions.
- Employing a large language model for 3D mesh generation.
- Auto-completing features at user-specified regions of the mesh.

We publish our code on GitHub and release two new datasets: quadrilateral versions of the triangle meshes from the DFAUST [1] and MANO [31] datasets.

2 Related work

Generative methods in computer graphics have been an active research field for many years. Before the rise in popularity of learning-based methods, geometric models were generated in a variety of ways, including L-systems [29], evolutionary methods [38], and model synthesis [20]. However, we focus on learning-based methods in the following, and we divide this class of methods into four different groups:

More recently, neural implicit surface representations have attracted significant attention [7, 12, 18, 21, 25, 28, 39]. In this type of representation, a neural network is trained to approximate a scalar and/or vector field such as the signed distance field of a shape whose surface is given implicitly as a level set of the learned function from which a mesh can be extracted using, e.g., Marching Cubes [19]. This type of representation is very versatile but struggles to capture thin, sharp features. Moreover, the generated meshes are typically quite dense even in regions with sparse features.

Another line of research focuses on generating 3D shapes indirectly. Some methods create a polygonal surface by conditioning on a point cloud, which can be generated using a diffusion model [13, 23, 34, 43]. For instance, Nichol et al. [23] and Zeng et al. [43] generate a point cloud, convert it to an implicit surface, and hence a mesh. In SpaceMesh [34], a transformer is used to predict the polygonal faces of a mesh that matches a given point cloud. The method generates a manifold mesh by construction since it is based on the halfedge data structure. However, the method is limited by its memory consumption and cannot generate meshes of more than 2000 vertices.

In a number of recent works, meshes are generated unconditionally by sampling autoregressively from a transformer. These works include Polygen [22], MeshGPT [37], MeshXL [4], MeshAnything V2 [5], and EdgeRunner [40].

Some of these can operate conditionally, but we focus on unconditional generation since this is more pertinent. The methods differ in their network architectures and in how they encode meshes into sets of tokens, but otherwise they build on the same principles. A mesh is predicted autoregressively, one primitive at a time, and space is discretized into a coarse grid that stores the vertices of the mesh. This is an artifact of the transformer network’s training, which outputs a probability distribution over a discrete set of tokens, as true continuous predictions perform poorly. Moreover, by predicting only one primitive at a time, the methods do not guarantee that the output meshes are manifold—unlike our method. Finally, all methods, with the exception of Meshtron [13], for which there is no published code yet, can only handle meshes with fewer than 4000 triangles. While these methods are the ones that most closely resemble our work, they differ significantly because we do not generate meshes at the primitive level but at the component level. This enables us to bypass the use of a 3D grid and makes the method insensitive to output resolution. In Table 1, we compare our method against three other state of the art transformer based methods with publicly available code.

LegoGPT [30], which produces shapes in units of blocks, is tangentially related to our work. Their method takes a 3D mesh, voxelizes it on a coarse grid to create a LEGO design, and then trains an LLM to assemble the shape from LEGO bricks. Despite the similarity in building shapes from components, our work is fundamentally different since we operate on meshes with unconstrained vertex positions. Furthermore, our extrusions adapt to the target patch, unlike LEGO bricks. The transformer-based tree generation method by Lee et al. [15] also shares similarities with our work. The authors quantize instructions for many L-systems and then train a transformer to generate various trees. This allows them to generate new trees by sampling from the transformer.

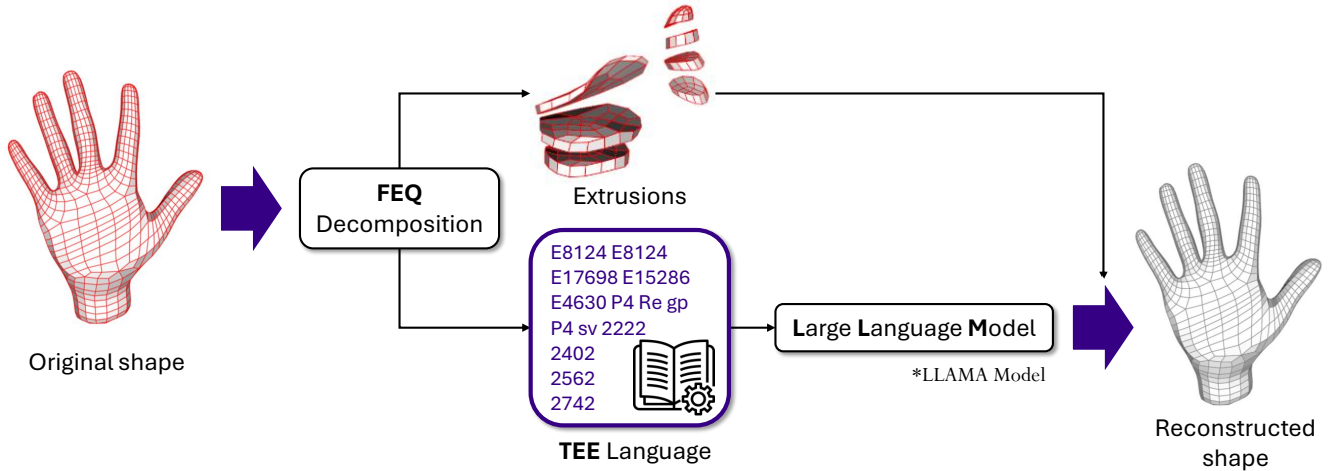


Figure 2: **Method overview:** Our method takes as input an FEQ mesh, which is decomposed into the individual face-loops and a building manual for assembling it again from its components.

Our work builds on the notion of Face Extrusion Quad (FEQ) meshes introduced by Pandey et al. [24]. FEQs are quad meshes with only non-intersecting face loops, i.e., no face is contained twice in the same face loop. Pandey et al. show that it is possible to decompose FEQ meshes and rebuild the same face loop structures from such recorded sequences. In this paper, we introduce a textual representation for extrusions and use an LLM to learn full extrusion sequences in terms of this representation.

Table 1: Comparison of capabilities across implicit methods, previous transformer-based mesh generators, and our LoopGPT approach.

	Implicit	Transformers	TEE
Sharp features	✗	✓	✓
Max number of faces	No limit	Up to 4000 [40]	No limit
Guaranteed manifold	✗	✗	✓
Continuous verts	✓	✗	✓
Feature completion	✗	✗	easy

3 Method

Inspired by Face Extrusion Quad (FEQ) meshes and the associated building methodology developed by Pandey et al. [24], we propose a framework for learning sequences of extrusions. The crucial observation is that extrusions can be described in terms of text, which, in turn, can be learnt by an LLM. This makes the extrusions malleable, allowing us to generate new extrusion sequences not in the examples used as training data.

In the following, we briefly define the main notions behind FEQ meshes and then describe our method, outlined in Figure 2.

FEQ Meshes. Given a quadrilateral mesh whose set of faces is denoted F , a *face loop* is a subset, $F_l \subset F$, which forms a contiguous ribbon (cf. Figure 3) such that each face is connected to its neighbors

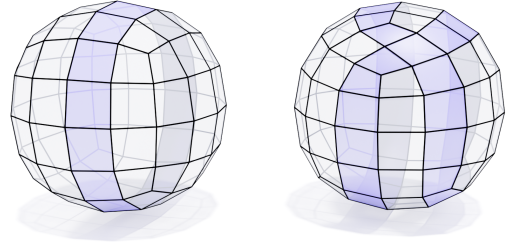


Figure 3: Two meshes, each with a single face loop highlighted in blue. The face loop on the right is self-intersecting.

in the loop by opposite edges called *sleeper edges*. The edges along the boundary of the face loop are called *rail edges*. We can traverse a face loop going from face to face across sleeper edges until we come back to the face from which we started. Any pure quad mesh, including non-FEQ meshes, is composed of *face loops*. To be precise, each face of any quad mesh belongs to either one or two face loops. If a face belongs to only one face loop, it is because it is contained twice in that loop which we then consider to be *self-intersecting* as shown in Figure 3. Non-self-intersecting face loops can be divided into self-adjacent and non-self-adjacent face loops. If two faces that both belong to the loop share an edge which is not a sleeper edge, it is said to be self-adjacent.

An extrusion is an operation on a set of faces, F_p , that has disk topology and which we denote the *base patch*. Disconnecting F_p from the rest of F results in two identical boundary edge cycles. The extrusion is completed by adding a face loop, F_l , that joins these two boundary cycles, which become its rails, reconnecting F_p to the rest of the mesh. The face set $F_p \cup F_l$ will be denoted the *extended base patch*. Importantly, extrusions are invertible operations, and the inverse is called a *face loop collapse*. The collapse of a face loop removes F_l and stitches the two rail curves to reconnect F_p with the rest of the mesh.

The face loop created by an extrusion is neither self-intersecting nor self-adjacent. This motivates the definition of an *FEQ mesh* as a closed, genus 0 quadrilateral mesh F without self-intersecting nor self-adjacent face loops. In the following, when we refer to face loops, it is understood that these are free of self-intersections and self-adjacency.

3.1 From Features to Extrusion Sequences

As Pandey et al. point out, we can build a feature of an FEQ mesh by applying a series of extrusions starting from a base patch on the original mesh. Since every extrusion builds on the previous extrusions, there is a clear hierarchical relationship between the extrusions. This relationship can be modeled with a directed acyclic graph (DAG), called the *extrusion graph*, whose nodes represent extrusions. An edge connects two nodes if the base patch of one (the child node) intersects the extended base patch of the other (the parent node). In other words, extrusions have a child-parent relationship if the child extrusion extrudes faces produced by the parent extrusion. Since face loops are produced by extrusions, we will use the word face loop when we focus on the result and extrusion when the operation is in focus.

A key idea in both Pandey et al. [24] and our work is that the features of FEQ meshes can be analyzed to identify extrusion sequences that could have generated them. We start by identifying *leaf nodes*. A leaf node is a face loop whose base patch contains no other complete face loops, i.e. $\neg\exists F'_l \subseteq F_l$. There are usually several leaf nodes to choose from, and we select the one with the smallest base patch area and collapse it. Once a leaf node has been collapsed, it exposes another face loop, which now becomes a leaf. Thus, we can run this process recursively until we arrive at the base patch for the entire feature. This is indicated by the collapse of the face loop marked by the user as the first face loop in the sequence. Note that at every collapse, we keep track of which face loops (or nodes) depend on the faces removed by the collapse. This is how we build the DAG that represents the FEQ feature.

Unlike Pandey et al., we need to linearize the DAG since it is converted to a text sequence. Topologically sorting the DAG yields a sequence of extrusions that one can follow to rebuild the part of the FEQ that was just decomposed. However, whenever the decomposed feature has a branching structure, there is no unique topological ordering of the extrusions. To make our method robust to the different ways a mesh can be generated, we augment our dataset with random topological orders for each decomposed part of the FEQ. However, only the branching nodes are topologically sorted, and we thus do not permute chains of extrusions, which only have *one* immediate successor and predecessor.

3.2 Applying Extrusion Sequences

With a topological ordering of a DAG from an FEQ mesh, we now have a sequence of extrusions to follow to build the FEQ part we decomposed. We select a set of quadrilateral faces from the mesh F as a base patch and choose an initial orientation based on a selected boundary vertex. With this, we can apply the first extrusion in the sequence to extrude the base patch. If the next extrusion in the sequence is a direct continuation of the first extrusion, we keep the orientation from the previous extrusion and use the extruded

face set from the first extrusion as the new base patch for the second extrusion. However, if extrusion $n + 1$ in the sequence only depends on a subset of faces in the base patch of extrusion n , or if extrusion $n + 1$ depends on faces from multiple previous extrusions k, l, \dots, m ($n > k, l, m$), we need to select the correct faces from these extrusion(s), which will form the base patch for extrusion $n + 1$. This selection is arguably the most challenging problem we had to solve. If we were to apply extrusions only to base patches of exactly the same connectivity as the original, we would simply need some method for labeling faces. However, as Pandey et al. did, we decided to apply extrusions to arbitrary base patches. To do so, we parametrize base patches both during decomposition and during the application of extrusion sequences. Next, for a given extrusion, we record the curves that enclose the regions to which the extrusion is applied in all involved extended base patches during decomposition. These curves are then used to find the regions to extrude in the parameter domains of the base patches during application.

3.3 Learning Extrusion Sequences

Our contribution hinges on the ability to learn extrusion sequences. While it would be possible to build a transformer model from scratch in order to learn the linearized representation of the extrusion graph, we opted instead for an approach that leverages the ability of modern LLMs to produce structured text.

To perform an extrusion, we need 1) a geometric description of the extruded base patch, 2) references to the previous extrusions we build upon, and, 3) for each of these, a curve that describes the extruded region. This information is converted to textual information for each extrusion in a sequence. We call this representation Text Encoded Extrusions (TEE).

Now, given a training set of different meshes, we can produce TEE strings for each feature that we decompose from a given mesh. This is sufficient for being able to store and apply extrusion sequences, but it would not generalize. In other words, we might hope that a language model could recall an extrusion sequence but not that it would be able to generate something new.

To achieve the ability to generate, we group the extrusions by applying each one onto a generic base patch, and then apply K-means clustering [26] on the vertex positions of the extruded patch, shown in Figure 6. For each cluster, the extrusion closest to the mean of the cluster becomes the cluster representative. Afterwards, all the extrusions in the building manuals are substituted with their cluster representative.

4 Implementation

In the following, we discuss the specifics of our approach to making extrusion sequences learnable. In Pandey et al., the authors delimit the region to be extruded by a closed curve. To allow a curve to cover the same region of a target base patch independently of the geometry of the patch, Pandey et al. computed a 2D harmonic map of the patch and described the boundary of the faces to be extruded (from the source patch) in this parameter domain. To determine the orientation, a vertex on the boundary was selected as a reference vertex and given the coordinates $(1, 0)$, after which the rest of the boundary vertices were mapped to the unit circle. With the boundary fixed, the interior vertices could be mapped to

the plane using the harmonic map, but, before computing the map, every quadrilateral face was split into four triangles by inserting a vertex at its center. To apply the extrusion, this parametrization method was also applied to the target patch, and faces whose center was inside the closed curve would be selected for extrusion.

We adopted this approach and used libigl [14] to compute the harmonic map of the extended base patch. Similar to Pandey et al. we only record the curves describing the base patch F_p of extrusion operation $n + 1$, if F_p consists of faces that come from multiple extended base patches of extrusions operations $j \in \{k, l, \dots, m\}$, $(n > k, l, m)$, or if F_p is a subset of faces from an extended base patch of only one extrusion operation j . In Pandey et al., the (u, v) coordinates of the curves describing the faces in F_p are stored together with the extrusion operation. However, to cluster the extrusion operations, we need to disentangle them from the curves describing the face sets F_p . Furthermore, as the LLM predicts a probability distribution over a discrete output space, the curves need to be discretized. We therefore introduce a generic extrusion (cf. Figure 4), which we use to discretize the curve. Essentially, the generic extrusion is a high-resolution mesh that covers the unit circle and therefore mimics the harmonic map of a base patch. It also has a face loop attached to the boundary of it. With this, every point in a curve with continuous (u, v) -coordinates can be mapped to the nearest vertex on the generic extrusion, and the curve thus becomes a sequence of vertex IDs. This is inherently discrete and, at the same time, provides generalization, as the vertex IDs can occur multiple times in TEE sequences. It also allows us to map back from a vertex ID on the generic extrusion to a 2D point on the circle.

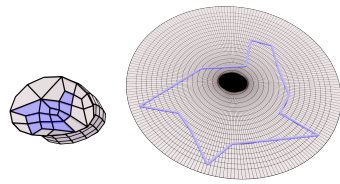


Figure 4: **Generic extrusion**: A set of faces highlighted in blue on an extended base patch to the left, and the boundary curve of the face set mapped to 2D and illustrated on the generic extrusion to the right

by inserting a new vertex at their center and connecting the new vertex to the boundary vertices of the face. Then the 3D-positions of the original vertices and the newly inserted vertices on the extended base patch are stored, after which the face loop is collapsed. The base patch is then flattened by smoothing the interior using Laplacian smoothing. The purpose of this step will be explained below. For each vertex in the smoothed base patch we then store the displacement vector from its current position to its previous position in the extended base patch.

Similar to Pandey et al., we want to be able to apply the extrusion operation to an arbitrary set of faces with disk topology. We therefore adopt their approach and compute a 2D parameterization of the base patch of the decomposed face loop, as this will allow us to compare it to the arbitrary set of faces for which we will also compute a 2D parameterization. Once again, we fix the boundary of the base patch to the unit circle and compute a harmonic map using [14]. The computation of the harmonic map was therefore also the motivation behind the smoothing step of the interior of the base patch during the decomposition. Consequently, each extrusion operation thus contains three things; namely, the displacement vectors, the (u, v) parameters of the vertices, and connectivity of the triangles $\{T_1, T_2, \dots, T_n\}$ in the base patch.

To apply the extrusion operation to a new base patch, we do the above decomposition procedure in reverse. We first smooth the interior of the base patch, and we then compute 2D parameterization using a harmonic map with the boundary of the new base patch fixed to the unit circle. Afterwards, we create a face loop and the extended base patch. Each vertex in the new extended base patch, therefore, has (u, v) -coordinates. These parameters will be used to find the enclosing triangle face T_i in the base patch of the extrusion operation. Once located, the displacement vectors of the vertices of T_i are interpolated using barycentric coordinates. To enhance robustness, the position of a vertex in the new extended base patch is computed by mapping the displacement vector to the reference frame of a boundary vertex in the new base patch and then averaging the computed displacements across all boundary vertices.

In Figure 5, an illustration of the application of the extrusion operation is seen. It is clear that different extrusions can yield very different results, as shown in Figure 6. Despite the differences in the extrusion operations, many of them have similar shapes - for instance the sequence of face loops making up a finger on a hand. This is what makes it possible to cluster the extrusions, crucial for the generalizability of our scheme.

The number of clusters directly affects the quality of reconstructions. For K equal to the number of extrusions in our dataset, we can perform lossless reconstructions. However, this comes at the

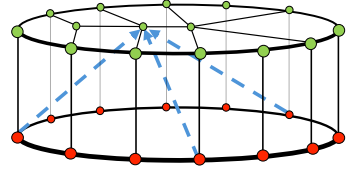


Figure 5: **Extruding the base patch**: The extrusion of the vertices in green of the extended base patch is determined by the extrusion vectors (blue) mapped to a local basis at each of the boundary vertices of the base patch (red).

4.1 Fetching the contributing base patches

When we generate a shape by applying each extrusion in the sequence, we also need the sequence to specify the necessary previous extrusions, and the closed loops, as intermediate steps, will need to be revisited. This representation should be discrete to align with the LLM's training scheme.

Specifying the previous extrusions, which we need later in the generation process, is, however, easy: we simply assign each applied extrusion a discrete sequential ID and store the extrusion with its ID in a database.

4.2 The Extrusion operation

Besides storing the closed loop defining the base patch of the face loop, the extrusion operation creating the face loop is also stored during the decomposition. This is done in the following way: First the quadrilateral faces of the extended base patch are triangulated

expense of generalization for the LLM. We choose the number of clusters K such that the loss in reconstruction quality is minimal. A comparison of the original shape and the shapes reconstructed with different numbers of clusters from our TEE is in Figure 7. As a tradeoff between generalization and visual quality, we choose $K = 20,000$.

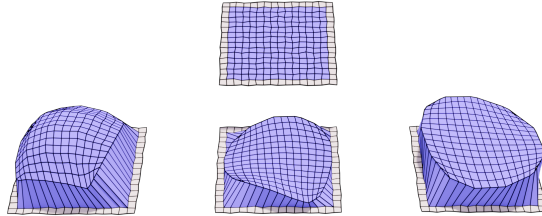


Figure 6: **Applying extrusions:** Three different extrusions are applied to the same base patch, creating three different extruded sets of faces.

4.3 Text Encoded Extrusions (TEE)

With the three elements in place: 1) a geometric description of the extruded base patch, 2) references to the previous extrusions we build upon, and 3) for each of these, a curve that describes the extruded region, we now have all the ingredients to build a FEQ-mesh. The only remaining thing is the recipe, which we call Text Encoded Extrusions (TEE). This recipe guides our framework in applying the extrusion sequence onto a set of faces with disk topology. An example of TEE is the sequence for the FEQ hand mesh in Figure 2 beginning with the structure:

E8124 E8124 E17698 E15286 E4630 P4 Re gp P4 sv
 2222 2402 2562 2742 ... (1)

Here, E8124 signals the application of extrusion 8124 from our dataset of extrusions to the selected base patch. We then apply extrusions sequentially until extrusion E4630, which we need to remember "Re" for future extrusions. We thus assign it an id (P4) and store the state of the mesh F , the sets of faces $\{F_p, F_l\}$ from the extrusion, and the harmonic map in a database with an ID corresponding to the number of extrusions applied so far. Since the next extrusion only needs a subset of faces from the previous extrusion, we fetch it from the database with gp signaling "get previous extrusion" and then the ID of the stored extrusion. We then use "sv" to signal that we select a set of vertices on the *generic extrusion*, which gets converted to (u, v) -coordinates of a closed loop. This closed loop is then used to select faces from $\{F_p, F_l\}$ that will become part of the base patch for the next extrusion.

4.4 Building methodology

Finding the appropriate faces on a mesh to apply an extrusion operation can be challenging if the connectivity of the base patch in the beginning of the extrusion sequence is very different from the connectivity of the original base patch of the extrusion sequence. The difference in connectivity causes the 2D parameterization of the

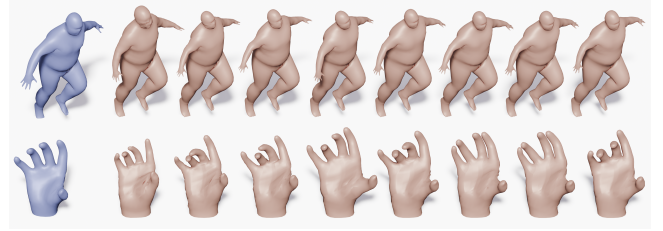


Figure 7: **TEE Reconstruction:** Clustering of the extrusions in the shape. Ground truth shapes (shown left in blue) and the reconstructions to the right. From left to right, the number of clusters is: 1k, 5k, 10k, 20k, 30k, 40k, 50k 60k.

new base patch to differ too much from the 2D parameterization of the original base patch on which extrusion operation was obtained. It therefore becomes a non-trivial problem to find the appropriate faces, as they may only be partially within a closed loop.

Consequently, we have developed two different building methodologies: A pure quadrilateral one and a quad-dominant approach. What sets the latter building methodology apart is the ability to cut through the base patch according to the loop denoting the faces needed for the extrusion. This cut might result in non-quadrilateral polygonal faces. We therefore triangulate these faces using a Delaunay triangulation using Triangle [36] while maintaining the edges making up the loop. No matter the building methodology, the extrusion sequence is the same. The result however can be quite different as illustrated in figure 8, where the shape on the left was reconstructed using the pure quadrilateral building methodology, and the one to the right with the quad dominant building methodology. For the quadrilateral-only method, we use a method inspired by flux to select a set of faces with disk topology, whose boundary curve matches the closed loop. For each edge, e , with vector e pointing from node u to node v , we compute a weight given by:

$$w(e) = \sum_{k=1}^K -\frac{e}{\|e\|} \cdot \frac{\mathbf{n}_{p_k}}{\|\mathbf{n}_{p_k}\|} + d_{p_k}^2 \quad (2)$$

Here \mathbf{n}_{p_k} is the normal of the line segment of the piecewise linear loop, which the point, p_k , sampled equidistantly on the edge vector e is closest to. d_{p_k} is the distance from the edge e to the line segment of the curve. With this weight function, we want to assign high values to edges that are orthogonal to their closest line segments and small weights to edges that are parallel. Moreover, we want to assign high values to edges, which are far away from their closest line segments, hence the addition of the squared distance. Once all edges have been assigned a weight, we sort them according to the lowest weights, and insert them into a tree until a cycle is detected. It should be noticed that it is not a minimum spanning tree, as we do not insert edges into the tree, if the edge is entirely within the closed loop. Afterwards we test the remaining edges and find their cycle. We then compare this cycle with the closed loop using Dynamic Time Warping [33], and select the cycle with the lowest value. This cycle then encloses a set of faces, and these will be a part of the base patch.

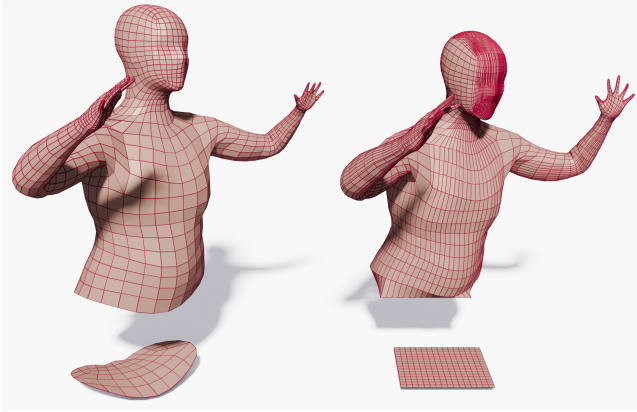


Figure 8: Building methodology: On the left, the torso is reconstructed from the standard body base patch, whereas a high-res square patch is used on the right.

4.5 LLM

To model our TEE, we use the Llama 3.2 1B model [8]. This model was chosen for its relatively large context window and its small number of parameters, which allow us to fine-tune it on our dataset. Since TEE is a text-based representation, fine-tuning an LLM on it can be done without modification of the LLM. As previously described, the core of our framework is not the neural network, but instead the geometric extrusion language, which generates a shape. Our method is thus agnostic to the LLM that is used.

5 Dataset

A dataset of FEQ meshes is essential for our method. These meshes must be 2-manifold, genus-0, quadrilateral, and free of self-intersecting face loops. Such meshes are difficult to obtain in practice.

Consequently, we use a combination of datasets, including surface meshes from the Hexalab dataset [2], a database of papers on hexahedral meshes. We filter out shapes that have triangles, self-intersecting loops, or a genus greater than 0. The authors of [24] also provided us with the FEQ meshes from their work. To diversify our FEQ meshes, we also created two additional FEQ datasets based on the MANO dataset (the right hands in the dataset) [31] and the DFAUST dataset (the upper parts of the bodies) [1]. We use an FEQ mesh of a hand and map the connectivity of this mesh to the triangle meshes in the MANO dataset using a bijective map computed between the FEQ hand mesh and one triangle mesh from the MANO dataset [32]. Similarly, we modify a human mesh from [3] to obtain an FEQ mesh. We then map this modified mesh to a humanoid from the DFAUST dataset using, again, a bijective mapping computed between these two meshes [32]. Since the DFAUST set contains time series of humans performing activities, we use a subset of meshes that are temporally distant to avoid including shapes that are very similar.

In total, we operate on three datasets: MANO, DFAUST, and a small highly diverse database of FEQ meshes generated using the skeleton-based conversion in Pandey et al. as well as surfaces extracted from hex meshes.

6 Results

Figure 9 shows qualitative results from our method, where the LLM was sampled with increasing levels of randomness, by modifying the temperature from 0.5 to 1.5 and top k (i.e. the number of tokens sampled among) from 5 to 100. Examples of hands generated with the same randomness are in Figure 10.

Figure 12 shows three meshes generated from our diverse dataset which do not resemble any single model and thereby demonstrate that the method has the ability to produce results that combine features from different parts of the training data.

6.1 Comparison with other methods

As previously stated, our method is orthogonal to prior work on LLM-based mesh generation, as we operate at the component level. This allows us to represent shapes with many more faces, which exceeds the limitations of the other works. We have compared our results against MeshXL [4], which is one of the most recent transformer based methods. To be able to generate results for MeshXL, we decimated the meshes to 500 faces and fine-tuned it on the MANO dataset. A qualitative comparison of the generated meshes is in Figure 11.

We also quantitatively evaluate the quality of the generated shapes using the Fréchet Inception Distance (FID), similar to [10]. We render the 3D meshes with smooth shading into 50k 2D images, with the camera positions uniformly distributed on a sphere around the object. Smooth shading enables a more fair comparison between meshes of lower numbers of faces. We compute the FID between the ground truth meshes rendered in this manner and 100 generated meshes from each dataset. On the MANO dataset, MeshXL [4] obtains an FID of 66.4, whereas our method obtains an FID of 13.23.

7 Discussions and limitations

As previously stated, our method assumes that the input 3D shapes are FEQ-meshes. These properties limit the data our method can train on, as most 3D datasets, such as ShapeNet, Objaverse, and Thingi10K, consist of triangle meshes. However, if an FEQ mesh is available, one can map that mesh onto similar meshes using a bijective map [32]. Moreover, a mesh with these properties is often a byproduct of a hexmesh, and generating hexmeshes is an active research field [27, 42], with databases such as [2]. Another limitation is the topology of the FEQ meshes. Currently, only FEQ meshes with spherical topology are supported, as meshes with a genus greater than zero complicate the linear ordering of the DAG. Moreover, not all extrusion directions are supported. If an extrusion branches in, our framework cannot decompose the mesh. Our model can also be challenged by very long extrusion sequences that branch, as approximation error accumulates.

8 Conclusion

We have presented a novel method for generating 3D shapes using an LLM. Our method is very different from previous approaches that construct meshes directly since we learn extrusion sequences rather than sequences of primitives. This allows us to generate both high- and low-resolution meshes. We are limited by the number of mesh features rather than the number of faces. Moreover, it allows for edits which is a crucial feature for designers.



Figure 9: Examples of generated meshes from the DFAUST dataset. The randomness during LLM sampling increases from left to right.



Figure 10: Examples of hand meshes generated by our method.



Figure 12: Three objects generated from extrusion sequences trained on a database of highly varied meshes. While the results are strange they demonstrate that the method is able to generate models that are very different from the training examples.



Figure 11: Comparison of hand meshes generated using MeshXL (top) and our method (bottom). To highlight key differences, the meshes are flat shaded and backfacing triangles are drawn red.

References

- [1] Federica Bogo, Javier Romero, Gerard Pons-Moll, and Michael J. Black. 2017. Dynamic FAUST: Registering Human Bodies in Motion. In *IEEE Conf. on Computer Vision and Pattern Recognition (CVPR)*.
- [2] Matteo Bracci, Marco Tarini, Nico Pietroni, Marco Livesu, and Paolo Cignoni. 2019. HexaLab.net: An online viewer for hexahedral meshes. *Cad Computer Aided Design* 110 (2019), 24–36. doi:10.1016/j.cad.2018.12.003
- [3] CG_Luke. 2016. LowPoly Base Mesh. In *Turbosquid*. <https://www.turbosquid.com/3d-models/lowpolygon-human-base-mesh-max-free/1049654>
- [4] Sijin Chen, Xin Chen, Anqi Pang, Xianfang Zeng, Wei Cheng, Yijun Fu, Fukun Yin, Zhibin Wang, Jingyi Yu, Gang Yu, Bin Fu, and Tao Chen. 2024. MeshXL: Neural Coordinate Field for Generative 3D Foundation Models. *Advances in Neural Information Processing Systems* 37 (2024).
- [5] Yiwen Chen, Yikai Wang, Yihao Luo, Zhengyi Wang, Zilong Chen, Jun Zhu, Chi Zhang, and Guosheng Lin. 2024. MeshAnything V2: Artist-Created Mesh Generation With Adjacent Mesh Tokenization. *Arxiv (cornell University)* (2024). doi:10.48550/arXiv.2408.02555
- [6] Zhiqin Chen, Andrea Tagliasacchi, Thomas Funkhouser, and Hao Zhang. 2022. Neural dual contouring. *Acm Transactions on Graphics* 41, 4 (2022), 3530108. doi:10.1145/3528223.3530108
- [7] Julian Chibane, Aymen Mir, and Gerard Pons-Moll. 2020. Neural Unsigned Distance Fields for Implicit Function Learning. *Advances in Neural Information Processing Systems* 33, *Neurips 2020* 33 (2020).
- [8] Abhimanyu Dubey, Abhinav Jauhri, Abhinav Pandey, Abhishek Kadian, Ahmad Al-Dahle, Aiesha Letman, Akhil Mathur, Alan Schelten, Amy Yang, Angela Fan, Anirudh Goyal, Anthony Hartshorn, Aobo Yang, Archi Mitra, Archie Srivankumar, Artem Korenev, Arthur Hinsvark, Arun Rao, Aston Zhang, Aurelien

Rodriguez, Austen Gregerson, Ava Spataru, Baptiste Roziere, Bethany Biron, Binh Tang, Bobbie Chern, Charlotte Caucheteux, Chaya Nayak, Chloe Bi, Chris Marra, Chris Mcconnell, Christian Keller, Christophe Touret, Chunyang Wu, Corinne Wong, Cristian Canton Ferrer, Cyrus Nikolaidis, Damien Allonsius, Daniel Song, Danielle Pintz, Danny Livshits, David Esiobu, Dhruv Choudhary, Dhruv Mahajan, Diego Garcia-Olano, Diego Perino, Dieuwke Hupkes, Egor Lakomkin, Ehab Albadawy, Elina Lobanova, Emily Dinan, Eric Michael Smith, Filip Radenovic, Frank Zhang, Gabriel Synnaeve, Gabrielle Lee, Georgia Lewis Anderson, Graeme Nail, Gregoire Mialon, Guan Pang, Guillen Cucurell, Hailey Nguyen, Hannah Korevaar, Hu Xu, Hugo Touvron, Iliyan Zarov, Imanol Arrieta Ibarra, Isabel Kloumann, Ishan Misra, Ivan Evtimov, Jade Copet, Jaewon Lee, Jan Geffert, Jana Vranes, Jason Park, Jay Mahadeokar, Jeet Shah, Jelmer Van Der Linde, Jennifer Billock, Jenny Hong, Jenya Lee, Jeremy Fu, Jianfeng Chi, Jianyu Huang, Jiawen Liu, Jie Wang, Jiecao Yu, Joanna Bitton, Joe Spisak, Jongsoo Park, Joseph Rocca, Joshua Johnstun, Joshua Saxe, Junteng Jia, Kalyan Vasudevan Alwala, Kartikeya Upasani, Kat Plawiak, Ke Li, Kenneth Heafield, Kevin Stone, Khalid El-Arini, Krithika Iyer, Kshitiz Malik, Kuenley Chiu, Kunal Bhalla, Lauren Rantala-Yearly, Laurens Van Der Maaten, Lawrence Chen, Liang Tan, Liz Jenkins, Louis Martin, Lovish Madaan, Lubo Malo, Lukas Blecher, Lukas Landzaat, Luke De Oliveira, Madeline Muzzi, Mahesh Pasupuleti, Mannat Singh, Manohar Paluri, Marcin Kardasz, Mathew Oldham, Mathieu Rita, Maya Pavlova, Melanie Kambadur, Mike Lewis, Min Si, Mitesh Kumar Singh, Mona Hassan, Naman Goyal, Narjes Torabi, Nikolay Bashlykov, Nikolay Bogoychev, Niladri Chatterji, Olivier Ducherine, Onur Celebi, Patrick Alrassy, Pengchuan Zhang, Pengwei Li, Petar Vasic, Peter Weng, Prajwal Bhargava, Pratik Dubal, Praveen Krishnan, Punit Singh Koura, Puxin Xu, Qing He, Qingxiao Dong, Ragavan Srinivasan, Raj Ganapathy, Ramon Calderer, Ricardo Silveira Cabral, Robert Stojnic, Roberta Raileanu, Rohit Girdhar, Rohit Patel, Romain Sauvestre, Ronnie Polidoro, Roshan Sumbally, Ross Taylor, Ruan Silva, Rui Hou, Rui Wang, Saghar Hosseini, Sahana Chennabasappa, Sanjay Singh, Sean Bell, Seohyun Sonia Kim, Sergey Edunov, Shaoliang Nie, Sharan Narang, Sharath Rarapthy, Sheng Shen, Shengye Wan, Shruti Bhosale, Shun Zhang, Simon Vandenhende, Soumya Batra, Spencer Whitman, Sten Sootha, Stephane Collot, Suchin Gururangan, Sydney Borodinsky, Tamar Herman, Tara Fowler, Tarek Sheasha, Thomas Georgiou, Thomas Scialom, Tobias Speckbacher, Todor Mihaylov, Tong Xiao, Ujjwal Karn, Vedanuj Goswami, Vibhor Gupta, Vignesh Ramathanan, Viktor Kerkez, Vincent Gouget, Virginie Do, Vish Venkatesh, Vladan Petrovic, Weiwei Chu, Wenhan Xiong, Wenyin Fu, Whitney Meers, Xavier Martinet, Xiaodong Wang, Xiaoqing Ellen Tan, Xinfeng Xie, Xuchao Jia, Xuewei Wang, Yaelle Goldschlag, Yashesh Gaur, Yasmine Babaei, Yi Wen, Yiwen Song, Yuchen Zhang, Yue Li, Yuning Mao, Zacharie Delpierre Couderet, Zheng Yan, Zhengxing Chen, Zoe Papakipos, Aadiya Singh, Aaron Grattafiori, Abha Jain, Adam Kelsey, Adam Shajnfeld, Adithya Gangidi, Adolfo Victoria, Ahuva Goldstand, Ajay Menon, Ajay Sharma, Alex Boesenberg, Alex Vaughan, Alexei Baevski, Allie Feinstein, Amanda Kallet, Amit Sangani, Anam Yunus, Andrei Lupu, Andres Alvaraldo, Andrew Caples, Andrew Gu, Andrew Ho, Andrew Poulton, Andrew Ryan, Ankit Ramchandani, Annie Franco, Aparajita Saraf, Arkabandhu Chowdhury, Ashley Gabriel, Ashwin Bharambe, Assaf Eiseman, Azadeh Yazdan, Beau James, Ben Maurer, Benjamin Leonhardt, Bernie Huang, Beth Loyd, Beto De Paola, Bhargavi Paranjape, Bing Liu, Bo Wu, Boyu Ni, Braden Hancock, Bram Wasti, Brandon Spence, Brani Stojkovic, Brian Gamido, Britt Montalvo, Carl Parker, Carly Burton, Catalina Mejia, Changhan Wang, Changkyu Kim, Chao Zhou, Chester Hu, Ching-Hsiang Chu, Chris Cai, Chris Tindal, Christoph Feichtenhofer, Damon Civin, Diana Beatty, Daniel Kreymer, Daniel Li, Danny Wyatt, David Adkins, David Xu, Davide Testuggine, Delia David, Devi Parikh, Diana Liskovich, Didem Foss, Dingkang Wang, Due Le, Dustin Holland, Edward Dowling, Eissa Jamil, Elaine Montgomery, Eleonora Presani, Emily Hahn, Emily Wood, Erik Brinkman, Esteban Arcuate, Evan Dunbar, Evan Smothers, Fei Sun, Felix Kreuk, Feng Tian, Firat Ozgenel, Francesca Caggioni, Francisco Guzmán, Frank Kanayet, Frank Seide, Gabriela Medina Flores, Gabriella Schwarz, Gada Bader, Georgia Swee, Gil Halpern, Govind Thattai, Grant Herman, Grigory Sizov, Guangyi, Zhang, Guna Lakshminarayanan, Hamid Shojanazeri, Han Zou, Hannah Wang, Hanwen Zha, Haroun Habeeb, Harrison Rudolph, Helen Suk, Henry Asperegn, Hunter Goldman, Igor Molybog, Igor Tufanov, Irina-Elena Veliche, Itai Gat, Jake Weissman, James Geboski, James Kohli, Japhet Asher, Jean-Baptiste Gaya, Jeff Marcus, Jeff Tang, Jennifer Chan, Jenny Chen, Jeremy Reizenstein, Jeremy Teboul, Jessica Zhou, Jian Jin, Jingyi Yang, Joe Cummings, Jon Carvill, Jon Shepard, Jonathan Mcphie, Jonathan Torres, Josh Ginsburg, Junjie Wang, Kai Wu, Kam Hou U, Karan Saxena, Karthik Prasad, Kartikay Khandelwal, Katayoun Zand, Kathy Matosich, Kaushik Veeraraghavan, Kelly Michelena, Keqian Li, Kun Huang, Kunal Chawla, Kushal Lakhota, Kyle Huang, Lailin Chen, Lakshya Garg, Lavender A, Leandro Silva, Lee Bell, Lei Zhang, Liangpeng Guo, Licheng Yu, Liron Moshkovich, Luca Wehrstedt, Madian Khabsa, Manav Avalani, Manish Bhatt, Maria Tsimpoukelli, Martynas Mankus, Matan Hasson, Matthew Lennie, Matthias Reso, Maxim Groshev, Maxim Naumov, Maya Lathi, Meghan Keneally, Michael L. Seltzer, Michal Valko, Michelle Restrepo, Mihir Patel, Mik Vyatskov, Mikayel Samvelyan, Mike Clark, Mike Macey, Mike Wang, Miquel Jubert Hermoso, Mo Metanat, Mohammad Rastegari, Munish Bansal, Nandhini Santhanam, Natascha Parks, Natasha White, Navyata

Bawa, Nayan Singhal, Nick Egebo, Nicolas Usunier, Nikolay Pavlovich Laptev, Ning Dong, Ning Zhang, Norman Cheng, Oleg Chernoguz, Olivia Hart, Omkar Salpekar, Ozlem Kalinli, Parkin Kent, Parth Parekh, Paul Saab, Pavan Balaji, Pedro Rittner, Philip Bontrager, Pierre Roux, Piotr Dollar, Polina Zvyagina, Prashant Ratanchandani, Pritish Yuvraj, Qian Liang, Rachad Alao, Rachel Rodriguez, Rafi Ayub, Raghatham Murthy, Raghu Nayani, Rahul Mitra, Raymond Li, Rebekkah Hogan, Robin Battey, Rocky Wang, Rohan Maheswari, Russ Howes, Ruty Rinott, Sai Jayesh Bondu, Samyak Datta, Sara Chugh, Sara Hunt, Sargun Dhillon, Sasha Sidorov, Satadru Pan, Saurabh Verma, Seiji Yamamoto, Sharadhi Ramaswamy, Shaun Lindsay, Shaun Lindsay, Sheng Feng, Shenghao Lin, Shengxin Cindy Zha, Shiva Shankar, Shuqiang Zhang, Shuqiang Zhang, Sining Wang, Sneha Agarwal, Soji Sajuyigbe, Soumith Chintala, Stephan Max, Stephen Chen, Steve Kehoe, Steve Satterfield, Sudarshan Govindaprasad, Sumit Gupta, Sungmin Cho, Sunny Virk, Suraj Subramanian, S. Y. Choudhury, Sydney Goldman, Tal Remez, Tamar Glaser, Tamara Best, Thilo Kohler, Thomas Robinson, Tianhe Li, Tianjun Zhang, Tim Matthews, Timothy Chou, Tzook Shaked, Varun Vontimitta, Victoria Ajayi, Victoria Montanez, Vijai Mohan, Vinay Satish Kumar, Vishal Mangla, Vlad Ionescu, Vlad Poenaru, Vlad Tiberiu Mihailescu, Vladimir Ivanov, Wei Li, Wencheng Wang, Wenwen Jiang, Wes Bouaziz, Will Constable, Xiaocheng Tang, Xiaofang Wang, Xiaojian Wu, Xiaolan Wang, Xide Xia, Xilun Wu, Xinbo Gao, Yanjun Chen, Ye Hu, Ye Jia, Ye Qi, Yenda Li, Yilin Zhang, Ying Zhang, Yossi Adi, Youngjin Nam, Yu, Wang, Yuchen Hao, Yundi Qian, Yuzi He, Zach Rait, Zachary Devito, Zef Rosnbrick, Zhaoduo Wen, Zhenyu Yang, and Zhiwei Zhao. 2024. The Llama 3 herd of models. (2024). doi:10.48550/arXiv.2407.21783

[9] Daoyi Gao, Yawar Siddiqui, Lei Li, and Angela Dai. 2024. MeshArt: Generating Articulated Meshes with Structure-guided Transformers. *arXiv preprint arXiv:2412.11596* (December 2024).

[10] Jun Gao, Tianchang Shen, Zian Wang, Wenzheng Chen, Kangxue Yin, Daiqing Li, Or Litany, Zan Cojic, and Sanja Fidler. 2022. Get3d: A generative model of high quality 3d textured shapes learned from images. *Advances in neural information processing systems* 35 (2022), 31841–31854.

[11] SFF Gibson. 1998. Constrained elastic surface nets: Generating smooth surfaces from binary segmented data. *Medical Image Computing and Computer-assisted Intervention - Miccai'98* 1496 (1998), 888–898.

[12] Benoit Guillard, Federico Stella, and Pascal Fua. 2022. MeshUDF: Fast and Differentiable Meshing of Unsigned Distance Field Networks. *Lecture Notes in Computer Science (including Subseries Lecture Notes in Artificial Intelligence and Lecture Notes in Bioinformatics)* 13663 (2022), 576–592. doi:10.1007/978-3-031-20062-5_33

[13] Zekun Hao, David W. Romero, Tsung-Yi Lin, and Ming-Yu Liu. 2024. Meshtron: High-Fidelity, Artist-Like 3D Mesh Generation at Scale. (2024).

[14] Alec Jacobson, Daniele Panozzo, et al. 2018. libigl: A simple C++ geometry processing library. <https://libigl.github.io/>.

[15] Jae Joong Lee, Bosheng Li, and Bedrich Benes. 2023. Latent L-systems: Transformer-based Tree Generator. *Acm Transactions on Graphics* 43, 1 (2023), 7. doi:10.1145/3627101

[16] Jiahao Li, Hao Tan, Kai Zhang, Zexiang Xu, Fujun Luan, Yinghao Xu, Yicong Hong, Kalyan Sunkavalli, Greg Shakhnarovich, and Sai Bi. 2024. INSTANT3D: FAST TEXT-TO-3D WITH SPARSE-VIEW GENERATION AND LARGE RECONSTRUCTION MODEL. *12th International Conference on Learning Representations, Iclr 2024* (2024).

[17] Chen Hsuan Lin, Jun Gao, Luming Tang, Towaki Takikawa, Xiaohui Zeng, Xun Huang, Karsten Kreis, Sanja Fidler, Ming Yu Liu, and Tsung Yi Lin. 2023. Magic3D: High-Resolution Text-to-3D Content Creation. *Proceedings of the Ieee Computer Society Conference on Computer Vision and Pattern Recognition 2023-* (2023), 300–309. doi:10.1109/CVPR52729.2023.00037

[18] Hsueh-Ti Derek Liu, Francis Williams, Alec Jacobson, Sanja Fidler, and Or Litany. 2022. Learning smooth neural functions via lipschitz regularization. *Siggraph22 Conference Proceeding: Special Interest Group on Computer Graphics and Interactive Techniques Conference Proceedings* (2022), 31 (13 pp.). doi:10.1145/3528233.3530713

[19] William E. Lorensen and Harvey E. Cline. 1987. Marching cubes: A high resolution 3D surface construction algorithm. *AcM Siggraph Computer Graphics* 21, 4 (1987), 163–169. doi:10.1145/37402.37422

[20] Paul Merrell and Dinesh Manocha. 2011. Model Synthesis: A General Procedural Modeling Algorithm. *IEEE Transactions on Visualization and Computer Graphics* 17, 6 (2011), 715–728. doi:10.1109/TVCG.2010.112

[21] Ben Mildenhall, Pratul P. Srinivasan, Matthew Tancik, Jonathan T. Barron, Ravi Ramamoorthi, and Ren Ng. 2022. NeRF: Representing Scenes as Neural Radiance Fields for View Synthesis. *Communications of the AcM* 65, 1 (2022), 99–106. doi:10.1145/3503250

[22] Charlie Nash, Yaroslav Ganin, S. M. Ali Eslami, and Peter W. Battaglia. 2020. PolyGen: An autoregressive generative model of 3D meshes. *37th International Conference on Machine Learning, Icml 2020* 168147–10 (2020), 7177–7186.

[23] Alex Nichol, Heewoo Jun, Prafulla Dhariwal, Pamela Mishkin, and Mark Chen. 2022. Point-E: A System for Generating 3D Point Clouds from Complex Prompts [arXiv]. *Arxiv* (2022), 8 pp.

[24] Karan Pandey, Karan Singh, and Jakob Andreas Bærentzen. 2022. Face Extrusion Quad Meshes. *Siggraph '22 Conference Proceedings* (2022), 10 (9 pp.). doi:10.1145/3528233.3530754

[25] Jeong Joon Park, Peter Florence, Julian Straub, Richard Newcombe, and Steven Lovegrove. 2019. DeepSDF: Learning continuous signed distance functions for shape representation. *Proceedings of the IEEE Computer Society Conference on Computer Vision and Pattern Recognition 2019-* (2019), 165–174. doi:10.1109/CVPR.2019.00025

[26] F. Pedregosa, G. Varoquaux, A. Gramfort, V. Michel, B. Thirion, O. Grisel, M. Blondel, P. Prettenhofer, R. Weiss, V. Dubourg, J. Vanderplas, A. Passos, D. Cournapeau, M. Brucher, M. Perrot, and E. Duchesnay. 2011. Scikit-learn: Machine Learning in Python. *Journal of Machine Learning Research* 12 (2011), 2825–2830.

[27] Nico Pietroni, Marcel Campen, Alla Sheffer, Giannmarco Cherchi, David Bommes, Xifeng Gao, Riccardo Scateni, Franck Ledoux, Jean Remacle, and Marco Livesu. 2022. Hex-Mesh Generation and Processing: A Survey. *ACM Trans. Graph.* 42, 2, Article 16 (Oct. 2022), 44 pages. doi:10.1145/3554920

[28] Ben Poole, Ajay Jain, Jonathan T. Barron, and Ben Mildenhall. 2023. DREAM-FUSION: TEXT-TO-3D USING 2D DIFFUSION. *11th International Conference on Learning Representations, ICLR 2023* (2023).

[29] P. Prusinkiewicz. 1986. Graphical applications of L-systems. *Proceedings of Graphics Interface '86 and Vision Interface '86* (1986), 247–253.

[30] Ava Pun, Kangle Deng, Ruixuan Liu, Deva Ramanan, Changliu Liu, and Jun-Yan Zhu. 2025. Generating Physically Stable and Buildable LEGO Designs from Text. *arXiv preprint arXiv:2505.05469* (2025).

[31] Javier Romero, Dimitrios Tzionas, and Michael J. Black. 2017. Embodied Hands: Modeling and Capturing Hands and Bodies Together. *ACM Transactions on Graphics, (Proc. SIGGRAPH Asia)* 36, 6 (Nov. 2017).

[32] P. Schmidt, D. Pieper, and L. Kobbelt. 2023. Surface Maps via Adaptive Triangulations. *Computer Graphics Forum* 42, 2 (2023), 103–117. doi:10.1111/cgf.14747

[33] Pavel Senin. 2008. Dynamic time warping algorithm review. *Information and Computer Science Department University of Hawaii at Manoa Honolulu, USA* 855, 1-23 (2008), 40.

[34] Tianchang Shen, Zhaoshuo Li, Marc Law, Matan Atzmon, Sanja Fidler, James Lucas, Jun Gao, and Nicholas Sharp. 2024. SpaceMesh: A Continuous Representation for Learning Manifold Surface Meshes. *Siggraph Asia 2024 Conference Papers* (2024). doi:10.1145/3680528.3687634

[35] Tianchang Shen, Jacob Munkberg, Jon Hasselgren, Kangxue Yin, Zian Wang, Wenzheng Chen, Zan Gojcic, Sanja Fidler, Nicholas Sharp, and Jun Gao. 2023. Flexible Isosurface Extraction for Gradient-Based Mesh Optimization. *ACM Trans. Graph.* 42, 4, Article 37 (jul 2023), 16 pages. doi:10.1145/3592430

[36] Jonathan Richard Shewchuk. 1996. Triangle: Engineering a 2D quality mesh generator and delaunay triangulator. *Lecture Notes in Computer Science (including Subseries Lecture Notes in Artificial Intelligence and Lecture Notes in Bioinformatics)* 1148 (1996), 203–222. doi:10.1007/bfb0014497

[37] Yawar Siddiqui, Antonio Alliegro, Alexey Artemov, Tatiana Tommasi, Daniele Sirigatti, Vladislav Rosov, Angela Dai, and Matthias Nießner. 2024. MeshGPT: Generating Triangle Meshes with Decoder-Only Transformers. *Proceedings of the IEEE Computer Society Conference on Computer Vision and Pattern Recognition* (2024), 19615–19625. doi:10.1109/CVPR52733.2024.01855

[38] K. Sims. 1994. Evolving virtual creatures. *Computer Graphics Proceedings. Annual Conference Series 1994. Siggraph 94 Conference Proceedings* (1994), 15–22. doi:10.1145/192161.192167

[39] Towaki Takikawa, Joey Litalien, Kangxue Yin, Karsten Kreis, Charles Loop, Derek Nowrouzezahrai, Alec Jacobson, Morgan McGuire, and Sanja Fidler. 2021. Neural Geometric Level of Detail: Real-Time Rendering with Implicit 3D Shapes. *Proceedings of the IEEE Computer Society Conference on Computer Vision and Pattern Recognition* (2021), 11353–11362. doi:10.1109/CVPR46437.2021.01120

[40] Jiaxiang Tang, Zhaoshuo Li, Zekun Hao, Xian Liu, Gang Zeng, Ming-Yu Liu, and Qinsheng Zhang. 2024. EdgeRunner: Auto-regressive Auto-encoder for Artistic Mesh Generation. (2024). doi:10.48550/arXiv.2409.18114

[41] Ashish Vaswani, Noam Shazeer, Niki Parmar, Jakob Uszkoreit, Llion Jones, Aidan N. Gomez, Łukasz Kaiser, and Illia Polosukhin. 2017. Attention Is All You Need. *Advances in Neural Information Processing Systems 30 (nips 2017) 30* (2017).

[42] P. Viville, P. Kraemer, and D. Bechmann. 2023. Meso-Skeleton Guided Hexahedral Mesh Design. *Computer Graphics Forum* 42, 7 (2023), e14932. doi:10.1111/cgf.14932

[43] Xiaohui Zeng, Arash Vahdat, Francis Williams, Zan Gojcic, Or Litany, Sanja Fidler, and Karsten Kreis. 2022. LION: Latent Point Diffusion Models for 3D Shape Generation. In *Advances in Neural Information Processing Systems (NeurIPS)*.